**Astronomy
&
Astrophysics**

H$_2$O in stellar atmospheres

U. G. Jørgensen[1], P. Jensen[2], G. O. Sørensen[3], and B. Aringer[4]

[1] Niels Bohr Institute, Astronomical Observatory, Juliane Maries vej 30, 2100 Copenhagen, Denmark
[2] Theoretische Chemie, Bergische Universität – Gesamthochschule Wuppertal, 42097 Wuppertal, Germany
[3] H. C. Ørsted Institute, Universitetsparken 5, 2100 Copenhagen, Denmark
[4] Institut für Astronomie der Universität Wien, Türkenschanzstraße 17, 1180 Wien, Austria

Abstract. We have performed a detailed ab initio computation of the dipole moment surface, the vibrational transition moments, and the spectral lines for the water molecule. A total of 412 vibrational eigenstates were identified below $30\,000$ cm^{-1}, corresponding to $\approx 85\,000$ vibrational transitions. In principle there are many billions of allowed vibration-rotation transitions between these eigenstates. In our most complete test calculations we constructed a list of 3 billion (3×10^9) lines. At room temperature, the computed monochromatic absorption coefficient is in good overall agreement with the HITRAN data base, while at higher temperatures its value exceeds the HITRAN-based absorption coefficient by more than an order of magnitude, due to the lack of high excitation lines in HITRAN. The agreement with the HITEMP version of HITRAN is considerably better than with the standard HITRAN. By comparing stellar model atmospheric structures and synthetic spectra based on our most extensive line list with results from calculations excluding the huge number of ultra-weak lines, we conclude that when the lines are well chosen, a few times 10 million lines are more than sufficient for all astrophysical purposes. We therefore offer to the community a line list of 100 million lines, easily accessible by anonymous ftp. Finally, we have compared results of synthetic stellar spectra based on this line list with observed ISO spectra and have found good agreement. In particular in the $2-4$ μm region around the strong fundamental bands, the agreement with observations is considerably better than that obtained with other available water line lists.

Key words. molecular data – astronomical data bases: miscellaneous – stars: atmospheres – stars: late-type – infrared: solar system – infrared: stars

1. Introduction

Water vapour has been known for a long time to play a very important role in cool stellar atmospheres, but older models were only able to give a rough estimate of the size of the effects (Auman 1967). An important step forward was the laboratory measurement of the integrated intensity at elevated temperatures by Ludwig et al. (1973) and the statistical treatment of these data to generate synthetic line data and opacity samplings from which more realistic model atmospheres were constructed, first by Brown et al. (1989) and later by Plez et al. (1992). The first models based on real line list data for H$_2$O were those of Jørgensen et al. (1994) based on a preliminary version of the present work. Later, several other models were constructed based on various versions of the list we present here, and full line list models were also constructed by Hauschildt et al. (1999); Allard et al. (2000) and others based on the NASA AMES line list by Partridge & Schwenke (1997).

Although several model atmospheres based on various, more or less preliminary versions of the present line list have been used in studies already published, our line list has never been properly finalised in a general, user-friendly form and presented in the literature. In the present work we therefore make up for this omission, and describe the "final" vibration-rotation line calculation, its organisation, and results of comparison with other line list data and with observed stellar spectra. The resulting line list is easily available to the community by anonymous ftp. It exists in three well documented forms particularly suitable for stellar opacity calculations, for spectroscopic studies, and for planetary analysis, respectively.

The original dipole moment calculations, potential energy surface, and vibrational transitions moment calculations also used for the present version of the line list, were described by Jørgensen & Jensen (1993). With the rapid evolution of computer capacity during recent years, it has now become feasible to test the construction of line lists with several different parameter settings of the rotational parameters, and test these against each other. In the most complete setting we tested a line list containing almost 3 billion lines. This list is, however, not

offered to the community other than in the form of an Opacity Sampling for the particularly interested reader, since it was soon realized that astrophysical calculations based on a few times 10 million lines are indistinguishable from the 3-billion-line-list results in all respects (except from the computing time). The three line lists that are made available are therefore a 100-million-lines list for high temperature opacity purposes (i.e. limited to information about gf values, excitation energies, and line strengths), a 1-million-lines list subsample with spectroscopic information for each line (quantum numbers etc.), and a 1-million-lines subsample particularly suitable for planetary atmospheric studies and other medium temperature studies.

In Sect. 2 we summarise the discussion of the vibrational band intensity calculations from the paper by Jørgensen & Jensen (1993) of relevance for the present study, in Sect. 3 we describe the calculation of the rotational transitions, in Sect. 4 we discuss the details of the line list itself, in Sect. 5 we compare the present work with other water line data in the literature, in Sect. 6 we analyse effects on the stellar atmospheric structure of H₂O opacities calculated under various assumptions, and finally in Sect. 7 we compare synthetic spectra with observed stellar spectra of cool giant stars rich in gaseous water.

2. The vibrational transitions

2.1. The dipole moment surface

The dipole moment surface was computed at the MC and at the CI level by use of the CASSCF theory (see e.g. Roos et al. 1980 or Langhoff & Bauschlicher 1994 for basic definitions). 8 active electrons in 8 active orbitals were considered. The basis set was a GTO 13s 8p 4d/8s 3p basis on oxygen/hydrogen, contracted to 8s 6p 4d/6s 3p, extended from the work of van Duijneveldt (1971). Experiments with an extra d-function on hydrogen gave no changes in the intensities. At the SCF level this basis set compared well with the results for an un-contracted 15s 8p 4d 1f/10s 3p 1d GTO test basis set, even for very large bend and stretch displacements. The energy in the equilibrium configuration was 0.0014 hartree above the theoretical Hartree-Fock limit.

We describe the dipole moment in terms of its coordinates $\bar{\mu}^{(p)}$ and $\bar{\mu}^{(q)}$ along axes p and q in the plane defined by the three nuclei. The q axis bisects the bond angle Θ and points so that the q coordinates of the two H nuclei (labelled 1 and 2, the O nucleus is labelled 3) are positive. The p axis is perpendicular to the q axis and points so that the p coordinate of nucleus 2 is positive. The function $\bar{\mu}^{(p)}$ is represented by the expansion

$$\bar{\mu}^{(p)} = \sum_{i,j,k} c_{ijk}^{(p)} \left(\cos\Theta - \cos\Theta_e\right)^i \Delta R_1^j \Delta R_2^k, \qquad (1)$$

where Θ_e is the equilibrium value of Θ and ΔR_m, $m = 1$ or 2, is the displacement from equilibrium of R_m, the

distance between the "terminal" H nucleus m and the O nucleus. Similarly, $\bar{\mu}^{(q)}$ is represented by

$$\bar{\mu}^{(q)} = \sin\Theta \sum_{i,j,k} c_{ijk}^{(q)} \left(\cos\Theta - \cos\Theta_e\right)^i \Delta R_1^j \Delta R_2^k. \qquad (2)$$

A set of dipole moment parameter values $c_{ijk}^{(p)}$ and $c_{ijk}^{(q)}$ was obtained by fitting the analytical functions through the dipole moment components resulting from the ab initio calculations. The resulting values are given in Tables 3 and 4 of Jørgensen & Jensen (1993), to which the reader is referred for more details on the calculation of the dipole moment surfaces.

2.2. The potential energy surface

The vibrational wavefunctions used for calculating the vibrational transition moments were generated with the MORBID (Morse Oscillator Rigid Bender Internal Dynamics) computer program (Jensen 1988). The potential energy function is expressed as

$$V(\Delta R_1, \Delta R_2, \Theta) = \sum_{i,j,k} f_{ijk} \left(\cos\Theta - \cos\Theta_e\right)^i y_1^j y_2^k, \qquad (3)$$

with

$$y_m = 1 - \exp\left(-a\,\Delta R_m\right), \qquad (4)$$

$m = 1$ or 2, where a is a molecular parameter. The values of the potential energy parameters f_{ijk} and a (and of the equilibrium bond lengths and bond angle) used in the present work were obtained by Jensen (1989) by fitting to experimental data.

In the MORBID approach, the rotation-vibration Hamiltonian is approximated by the sum of the potential energy function given in Eq. (3) and an approximate kinetic energy operator obtained as a fourth order expansion in the y_m's and in the conjugate momenta $\widehat{P}_m = -i\hbar\partial/\partial\Delta R_m$. The eigenvalues and eigenfunctions of this Hamiltonian are calculated by diagonalization of a matrix representation for it; the vibrational basis set used is a product of

1. stretching functions $|N_{\text{vib}}\Gamma_{\text{Sym}}\rangle$, obtained as the eigenfunctions of the Hamiltonian $\widehat{H}_{\text{Stretch}}$ (Eq. (58) of Jensen 1988) which describes the molecule in question stretching with its bond angle fixed at the equilibrium value Θ_e. The index N_{vib} characterises the zeroth order stretching state, and Γ_{Sym} is the irreducible representation spanned by the function $|N_{\text{vib}}\Gamma_{\text{Sym}}\rangle$ in the appropriate molecular symmetry group (Bunker & Jensen 1998), and

2. bending basis functions $|v_2, K\rangle$ (see Sect. 5 of Jensen 1988) as eigenfunctions for the Hamiltonian $\widehat{H}_{\text{Bend}}$ (Eq. (63) of Jensen 1988) describing the molecule bending and rotating around the molecule-fixed axis of least moment of inertia with its bond lengths fixed at the equilibrium values R_1^e and R_2^e. The index v_2 is the bending quantum number for a bent triatomic molecule.

The eigenfunctions of the Hamiltonian for the complete molecule are by the good quantum numbers J, M, and Γ_{rv}, where $M\hbar$ is the projection of the total angular momentum on the space-fixed Z-axis and Γ_{rv} is the symmetry of the wavefunction, together with an index i numbering the states with common values of (J, M, Γ_{rv}). We approximate such an eigenfunction as

$$|i; J, M, \Gamma_{rv}\rangle = \sum_{N_{\mathrm{vib}}, \Gamma_{\mathrm{Sym}}, v_2, K} c^{(i; J, M, \Gamma_{rv})}_{N_{\mathrm{vib}}, \Gamma_{\mathrm{Sym}}, v_2, K}$$
$$\times |N_{\mathrm{vib}} \Gamma_{\mathrm{Sym}}\rangle |v_2, K\rangle |J, K, M\rangle \qquad (5)$$

where $|J, K, M\rangle$ is a usual rigid rotor eigenfunction (Bunker & Jensen 1998) and the expansion coefficients $c^{(i; J, M, \Gamma_{rv})}_{N_{\mathrm{vib}}, \Gamma_{\mathrm{Sym}}, v_2, K}$ are determined through matrix diagonalization. In the present section we are only concerned with states having $J = 0$.

For vibrational states whose energy has been experimentally measured, our calculated vibrational energy is generally within a few cm^{-1} of the corresponding experimental value. For a detailed comparison of rotation-vibration energy levels obtained with the potential energy surface used in the present work with experimental results, see Jensen (1989) or Fernley et al. (1991).

2.3. Integrated band intensities

We obtain the matrix elements of the dipole moment components in Eqs. (1) and (2) between the eigenfunctions of Eq. (5) as

$$\langle i'; J', M', \Gamma'_{rv} | \bar{\mu}^{(\alpha)} | i; J, M, \Gamma_{rv}\rangle$$
$$= \sum_{N'_{\mathrm{vib}}, \Gamma'_{\mathrm{Sym}}, v'_2, K'} \left(c^{(i'; J', M', \Gamma'_{rv})}_{N'_{\mathrm{vib}}, \Gamma'_{\mathrm{Sym}}, v'_2, K'} \right)^*$$
$$\times \sum_{N_{\mathrm{vib}}, \Gamma_{\mathrm{Sym}}, v_2, K} c^{(i; J, M, \Gamma_{rv})}_{N_{\mathrm{vib}}, \Gamma_{\mathrm{Sym}}, v_2, K} \qquad (6)$$
$$\times \langle N'_{\mathrm{vib}} \Gamma'_{\mathrm{Sym}}; v'_2; J', K', M' | \bar{\mu}^{(\alpha)} | N_{\mathrm{vib}} \Gamma_{\mathrm{Sym}}; v_2; J, K, M\rangle,$$

$\alpha = p$ or q. The calculation of the matrix elements on the right hand side of Eq. (6) is described in Jensen (1988). If we assume the molecules to be in thermal equilibrium at the absolute temperature T, we obtain the vibrational band intensities S_{v}^0 as

$$S_{\mathrm{v}}^0 = \left(\frac{8\pi^3}{3hc} \right) \nu_0 \, N_A \, \frac{\exp\left(-\frac{E_L}{kT}\right) \left(1 - \exp\left(-\frac{\nu_0 hc}{kT}\right)\right)}{Q_{\mathrm{v}}(T)}$$
$$\times \left| \langle i'; 0, 0, \Gamma'_{rv} | \bar{\mu}^{(\alpha)} | i; 0, 0, \Gamma_{rv}\rangle \right|^2, \qquad (7)$$

where the matrix element is given by Eq. (6) with $J' = J = M' = M = 0$, $\alpha = q$ if $\Gamma'_{rv} = \Gamma_{rv}$ ($= A_1$ or B_2) and $\alpha = p$ if $\Gamma'_{rv} \neq \Gamma_{rv}$. In Eq. (7), h is Planck's constant, c is the vacuum speed of light, ν_0 is the wavenumber of the vibrational transition, E_L is the energy of the lower state, k is the Boltzmann constant, N_A is Avogadro's number, and $Q_{\mathrm{v}}(T)$ is the vibrational partition function which depends on the absolute temperature T.

Our results for the intensities of the stronger bands generally agree with recent laboratory values to within a few percent. For the strongest fundamental mode (the bending mode at $6\,\mu$m) our result is 73 km mol^{-1} compared to 61 ± 6 km mol^{-1} for the average of seven recent experimental values. For the two stretching modes (both close to $2.7\,\mu$m) our results are 45.4 km mol^{-1} and 2.12 km mol^{-1}, while the laboratory values listed in the HITRAN data base are 43.4 km mol^{-1} and 2.98 km mol^{-1}, respectively. These agreements are comparable to or better than the most accurate other results found in the literature. A detailed description of our derived integrated band intensities, and a comparison of these with laboratory measurements, were given by Jørgensen & Jensen (1993).

The average intensity of our computed combination bands follow the experimental values through the 9 orders of magnitude in the intensity reported on in the literature (Rothman et al. 1987, 1998), although, as expected, with a bigger scatter for the weaker bands. Most of the scatter in our data can be explained as pairs of bands which have similar experimental values for their band center frequencies, and therefore suffer from energy level mixing and corresponding intensity borrowing. For such pairs, our calculated intensity is higher than the experimental value for one member and lower for the other member, whereas there is a good agreement with the experiments for the average values of such pairs. In practice, the effect on the total opacity and on the stellar atmospheres will therefore be only marginal, because the effective frequency shift of the combined intensity of a pair, is very small compared to the overall spectral energy distribution.

When disregarding the effective intensity shift between such nearby pairs of bands, our computation of the band strengths are therefore in agreement with laboratory measured intensities to within the accuracy in the laboratory intensities over the complete 9 orders of magnitudes in intensity range covered by existing laboratory measurements.

If the discrepancies within pairs of bands are due to incomplete correction for intensity borrowing in the experimental intensities, use of the experimental intensities as input data for fitting of an empirical dipole moment surface would clearly lead to erroneous values of the resulting "fitted" intensities. This might be the explanation for the less accurate results obtained by fits to observed intensities (e.g., Iachello & Oss 1990), compared to our theoretically based intensities.

Our computations predict many undiscovered bands in the visual and near ultraviolet part of the spectrum with intensities comparable to the experimentally known bands at longer wavelengths, which has strong implications for astrophysics as well as for climate research.

3. The rotational line transitions

The rotational lines including intensities were computed using conventional rigid-rotor theory. The rotational

spectrum of water has been extensively studied in the laboratory at ambient temperatures. For the lower vibrational levels the observed lines can be fitted quite well using a standard Hamiltonian (see, for example, Sarka & Demaison 2000), which, however, must be expanded to include high orders of centrifugal distortion terms. At the high temperature and low intensity limit required in the present calculations we reach so high J-values that this type of expansions diverge, and centrifugal distortion corrections were therefore neglected in producing the line list. The rotational constants of the higher vibrational levels were estimated by using a linear expansion in the harmonic quantum numbers.

$$B_v = B_0 + \sum_i \alpha_i^B v_i \qquad (8)$$

where B_0 is a rotational constant of the vibrational ground state.

Table 1. Adopted parameters (cm^{-1}) for expanding rotational constants.

Rot. Const.	B_0	α_1^B	α_2^B	α_3^B
A	27.8806	0.495	–3.2488	1.234
B	14.5218	0.224	–0.1655	0.112
C	9.2777	0.145	0.1488	0.169

This procedure will of course not automatically ensure a desired accuracy for line identification in high resolution spectroscopy, which is not the primary aim of our list. For such purposes, however, laboratory line lists (for example HITRAN; Rothman et al. 1998) exist, which can be used alone or in combination with the SCAN H₂O list.

4. The SCAN H₂O line list

The list of vibrational-rotational lines for H₂O, computed as described above, is available to the community as part of the SCAN line list data base (Jørgensen 1995, 1997). Experience with computation (and use in stellar astronomy) of line list data for other molecules has taught us that it is crucial for the resulting stellar atmosphere, and for the computed synthetic spectra, that the line list be as complete as possible (see for example Jørgensen & Larsson 1990).

For the diatomic molecules in the SCAN data base line list, the completeness has been assured by computing basically all allowed transitions with excitation energy up to the dissociation limit. For CN, for example, this procedure led to a list of 4 million lines (Jørgensen & Larsson 1990).

For H₂O this approach is not possible because, in principle, it would lead to a listing of billions of lines ($\approx 85\,000$ vibrational transitions $\times$ a few hundred rotational levels per band $\times$ the existing branches $\times$ a large number of different values of Δk for each vib-rot transition). As will

Table 2. Partition functions for H₂O at temperatures (first column) between 1000 K and 6000 K computed as a summation of the MORBID energy levels (Col. 2), as a summation of second order anharmonic energy levels up to $40\,000$ cm^{-1} (Col. 3), and as derived from the standard analytical expression from harmonic oscillator theory (Col. 4).

Temp.	Q_{Morbid}	$Q_{40\,000}$	Q_{harmonic}
1000.	1.1239	1.1239	1.1230
2000.	1.7085	1.7084	1.6925
3000.	2.7886	2.7853	2.7095
4000.	4.4637	4.4571	4.2256
5000.	6.8499	6.8786	6.3191
6000.	10.0225	10.2293	9.0769

be shown in the following section, for applications of the line list it is – fortunately enough – sufficient to consider only a few times 10 million lines.

The procedure of ensuring that sufficiently many vibrational levels are considered has been the same as used for the previous lists. To ensure that sufficiently many rotational transitions are included for each band, we include increasingly weaker lines (at 3500 K) until a convergence in the model atmosphere structure and the synthetic spectrum is reached. This procedure will ensure inclusion of enough lines to exceed the computational (and measurable) accuracy for the integrated opacity, model structures, and low resolution spectroscopy, for high temperature gas conditions (and hence for any conditions).

In order to consider all vibrational transitions up to the dissociation energy ($\approx 40\,000$ cm^{-1}), it would be necessary to consider energy levels with quantum numbers up to $(v_1, v_2, v_3)_{\mathrm{max}} \approx (12, 40, 12)$ (estimated from use of second order molecular constants fitted to measured energy levels). In our computation we considered all energy levels up to $(v_1, v_2, v_3)_{\mathrm{max}} = (8, 18, 7)$. This choice ensures that energy levels corresponding to $\approx 98\%$ of the vibrational partition function for temperatures up to 6000 K are included in the computation. We will say that in this sense the band list is 98% complete. Our relative choice of maximum quantum numbers is internally slightly inconsistent, in the sense that the stretching levels are computed to higher energies than the bending levels, but it still ensures a very high degree of completeness, and ensures that the considered vibrational transitions are reduced from $1213^2/2 \approx 736\,000$ (1213 being the number of energy levels with $E < 40\,000$ cm^{-1}), to $412^2/2 \approx 85\,000$.

We show in Table 2 the vibrational partition function as derived from a summation of the MORBID energy levels, from a summation of all energy levels with $E < 40\,000$ cm^{-1} (computed by use of second order molecular constants), and as the standard analytical formula derived from the harmonic oscillator approximation, $Q^{-1} = \prod(1 - \exp(-\omega\,hc/kT)^d)$. The fact that the partition function is smaller for $T = 2000$ K to 4000 K

when summed over all anharmonic energy levels up to $40\,000$ cm^{-1} than when summed over the MORBID energy levels up to $30\,000$ cm^{-1}, reflects that the MORBID energy levels and the anharmonic molecular constant energy levels are not identical for low vibrational quantum numbers. The MORBID approximation gives a better fit to the observed energy levels. For these temperatures we will therefore say that the partition function is 100% complete within the uncertainty in the determination of the energy levels.

In stellar atmospheres the partial pressures of H₂O are negligible above $T \approx 4000$ K, and our vibrational band calculation is therefore 100% complete for stellar atmosphere computations in the sense described above.

5. Comparison with other line lists for H₂O

5.1. The HITRAN data base

The latest version of the HITRAN data base (Rothman et al. 1998) includes data for $47\,716$ lines of ^{1}H$_2^{16}$O from 86 vibrational transitions. Of these bands, 72 are from the vibrational ground level (000), while 14 bands are hot bands of some of these, from vibrational states with $v_1 v_2 v_3 =$ levels 010 or 020. Typically, the highest rotational quantum number encountered for each band is around $J_{\max} = 10$ ($J_{\max}$ from 3 to 20). This listing is highly valuable for spectroscopic identification of strong lines in stellar spectra, and for construction of absorption coefficients at temperatures close to room temperature. For the higher temperatures often encountered in astrophysical situations, this listing is insufficient for construction of the absorption coefficient.

In Fig. 1 we compare the absorption coefficient calculated based on the HITRAN data base line list and based on our line list. Both absorption coefficients are calculated by folding each line with a Gausian profile with a half-width of 3 km s^{-1}. Lower panel is for $T = 296$ K, middle panel for $T \approx 1600$ K, and upper panel is for $T \approx 3900$ K. It is immediately seen that while there is a good overall agreement between the two lists at room temperature, the integrated absorption coefficient due to our list divided by the corresponding number for the HITRAN list increases rapidly with temperature. This is an effect of the lack of hot bands starting in higher excited states, weak bands in general, and lines with high rotational quantum number, in the HITRAN listing. At 3900 K the ratio of the two absorption coefficients, integrated over the spectral interval shown in Fig. 1, is approximately 20. This means that lines accounting for 95% of the integrated absorption coefficient (at this temperature) are missing in the HITRAN line list.

The data base HITEMP is a high temperature extension of the HITRAN data base for the molecules H₂O, CO₂, and CO. It includes almost 1.3 million lines for H₂O. At 3900 K the integrated absorption coefficient is 3 times larger than the one from HITRAN. At 1600 K the integrated absorption coefficient of the two compilations differ by only 4%, but
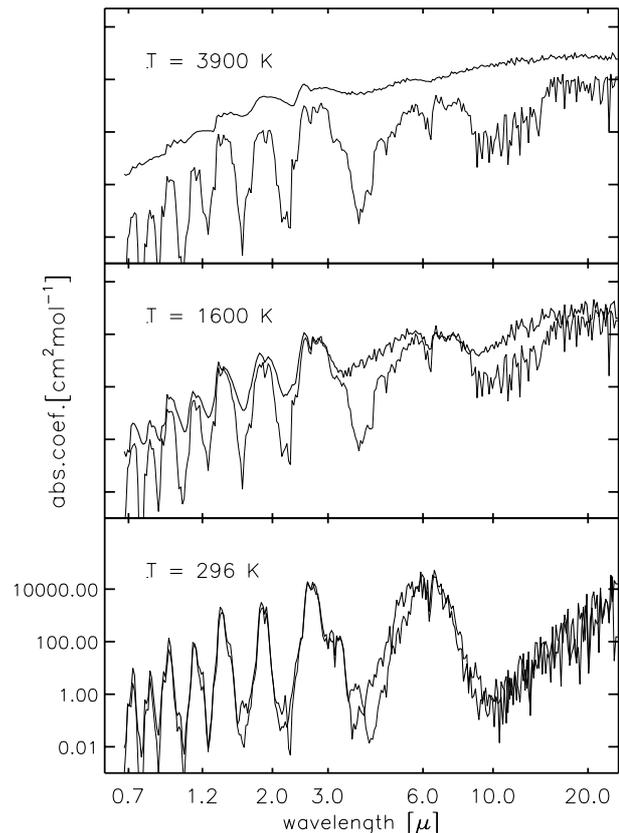
Fig. 1. Comparison of absorption coefficients calculated from the line list data in HITRAN (thin lines) and in the present work (thick lines), at the three different temperatures given in the panels.

the main difference is the many weak lines included in the HITEMP list, which result in a much higher absorption coefficient inbetween the strong absorption bands, with important implications for stellar spectrum synthesis. This list is highly recommendable for identification of individual vibration-rotation lines in stellar spectra. Since it is a direct compilation of laboratory data, it has a much better accuracy in the frequencies of individual lines than our computed line list, and yet it contains probably all lines that will be individually visible in stellar spectra. It is often forgotten in analysis of stellar spectra that also the laboratory measurements of weak lines have quite a large uncertainty in the estimated absolute value of the intensity. For quantitative stellar analysis it is therefore recommendable to consult several estimates of the gf-values, and in this sense our list and the HITEMP list are important complements, because the HITEMP list relies completely on measured values, while our list relies solely on computed values, and this is the basic reason why we offer also a small 1-million-lines list for spectroscopic identification although it will be inferior to the HITEMP list concerning the line positions. Figure 2 compares the low resolution integrated absorption coefficient of the HITEMP data with corresponding results from our full line list compilation.
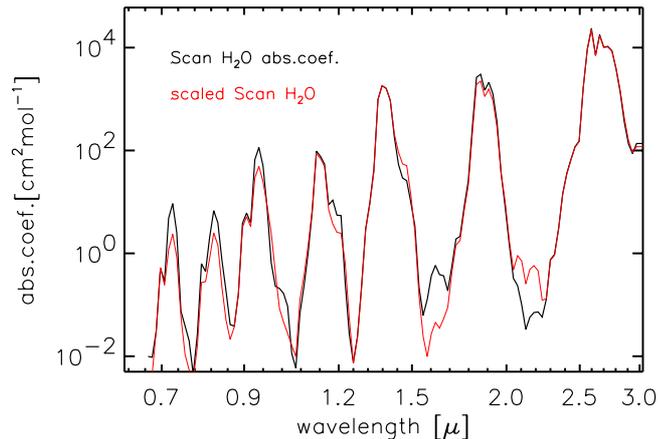
In a previous paper (Jørgensen & Jensen 1993) we compared the integrated room-temperature absorption
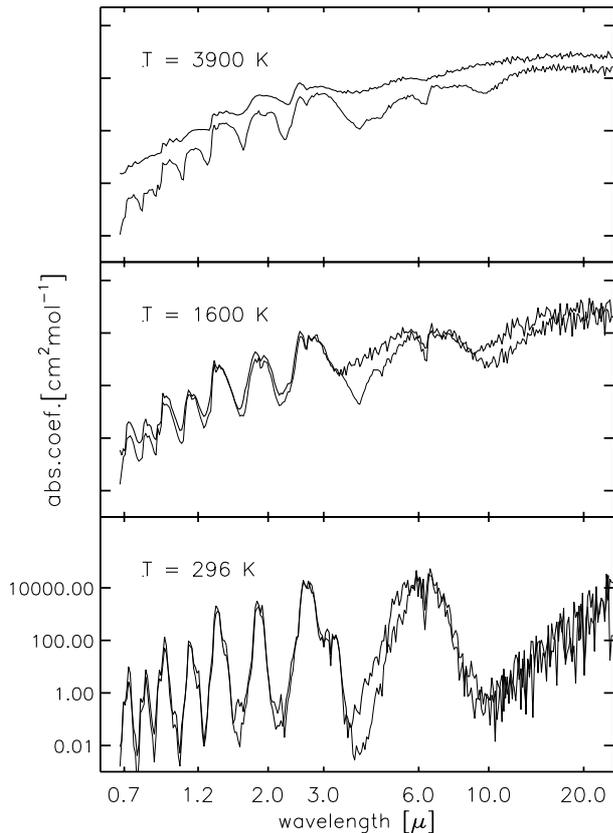
Fig. 2. Comparison of absorption coefficients calculated from the line list data in HITEMP (thin lines) and in the present work (thick lines), at the three different temperatures given in the panels.


Fig. 3. Absorption coefficients at 296 K calculated with (thin grey line) and without (thick black line) scaling (as described in the text) to the band intensities given in the HITRAN data base.

coeffcients of all bands listed in the HITRAN data base with the corresponding numbers from our list. For the stronger bands the general agreement is within a few percent, while typical ratios between our band intensity values and those from HITRAN (at room temperature) vary from 0.3 to 3 for the very weakest bands, which are up to 9 orders of magnitude weaker than the fundamental bands. The agreement for pairs of possible intensity mixed bands is considerably better than for individual bands, as described above. The uncertainty is probably within the uncertainty of the laboratory measurements, judged from the results of independent measurements where available. The uncertainty in the ab initio intensities are very hard to judge other than from comparison with laboratory measurements.

While it is therefore not obvious that the derived values from laboratory measurements are more "correct" than the theoretically derived ones, we experimented with the results of scaling all bands in our calculation to the values listed in the HITRAN data base. At least this procedure will give some kind of estimate of the uncertainty of the computed monochromatic absorption coefficient. The scaling was done by first determining the ratios of our values for the temperature independent band strengths (i.e., the vibrational transition moments) to those of HITRAN for the 72 bands in the HITRAN list that originate from the vibrational ground state. It was assumed that this ratio is

constant for all hot bands of a given band. With this assumption, the monochromatic absorption coefficient was calculated for all the 72 bands and their hot bands at all temperatures. This absorption coefficient was then complemented with the pure ab initio results for the bands that have no listing in HITRAN. In this way the bulk of the absorption coefficient has been scaled.

The result of the scaling is shown in Fig. 3 for the spectral interval from 0.7 to 3.0 μm. At longer wavelengths (where the integrated absorption coefficient is dominated by few strong vibrational bands) the two absorption coefficients are indistinguishable on a plot of the scale of Fig. 3. The two most pronounced differences in the figure are for the weak bands near 1.6 μm and near 2.2 μm. However, being in the weak part of the absorption coefficient, the final computed spectrum in these two regions are sensitive also to other molecular absorbers, and to the quality of the continuum drawing.

The major difference near peaks of the monochromatic absorption coefficient is seen to be for the three bands near 0.7, 0.8, and 0.9 μm. In most stellar objects cool enough to show signatures of water, this region of the spectrum is, however, dominated by strong bands of TiO, and these water bands are therefore hardly visible. The most pronounced difference between scaled and non-scaled results for normal stellar spectra therefore ends up being the strong band centered around 1.9 μm. The two strongest vibrational transitions in this region are the 011 and the 110 combination bands, with intensities at room temperature of 4.84 km mol^{-1} and 0.224 km mol^{-1} according to HITRAN and of 6.65 km mol^{-1} and 0.143 km mol^{-1} from our calculation.

While Fig. 3 shows the effect on the monochromatic absorption coefficient, Fig. 4 shows the corresponding effect on the resulting spectra for a stellar atmospheric model of $T_{\rm eff} = 3000$ K, $\log g = 0.0$, and solar metallicity. Obviously, the intensity of the scaled spectral feature around 1.9 μm is slightly weaker than the un-scaled one. The magnitude
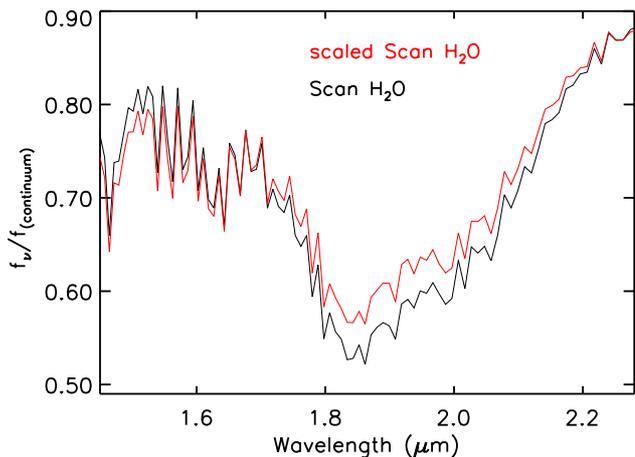
Fig. 4. The synthetic spectrum of a $T_{\rm eff} = 3000$ K, $\log g = 0$ stellar model in the region 1.5 to 2.3 μm. Black line is a spectrum computed directly from the Scan H$_2$O line list, while the grey line is a corresponding computation where bands have been scaled to their listed values in the HITRAN data base, as in Fig. 3.

of the effect is, however, seen to be relatively small, and it is for the moment not clear which of the two predicted spectra is in best agreement with stellar observations.

5.2. The NASA AMES list and the University-College-London list

After we had first announced our line list calculation (Jørgensen & Jensen 1993; Jørgensen et al. 1994), a similar calculation was performed at NASA AMES (Partridge & Schwenke 1997) based on the same (CASSCF) ab initio theory as in our calculation. The main difference between our calculation and the NASA AMES calculation (hereafter the PS97 list) is that the PS97 list include more observational data from the HITRAN data base into the list. The main philosophy behind this inclusion was to first compute the potential purely ab initio and then adjust it until an optimal fit to the line frequencies in the HITRAN line list was obtained. The main advantage of this procedure is that the line frequencies agree with laboratory work, while the main disadvantage is that possibly misidentifications and other uncertainties in the laboratory work to a large degree are transferred into the theoretical results.

In Fig. 5 we compare the monochromatic absorption coefficient calculated from our own list with that obtained from the PS97 list. At room temperature (lowest panel in Fig. 5) we recognize the differences seen also in Fig. 3 (the peaks near 0.7, 0.8, and 0.9 μm, and the minima near 1.6 and 2.1 μm), while another major difference is in the $4-5\,\mu$m region. In particular the $4-5\,\mu$m discrepancy can be traced to the higher temperatures in the two upper panels ($T \approx 1600$ K and $T \approx 3900$ K). At high temperatures also the discrepancies around $10\,\mu$m and at wavelengths shorter than $\approx 1\,\mu$m become pronounced. In Sect. 7 below, we compare results from both line lists with observed spectra from the ISO satellite.
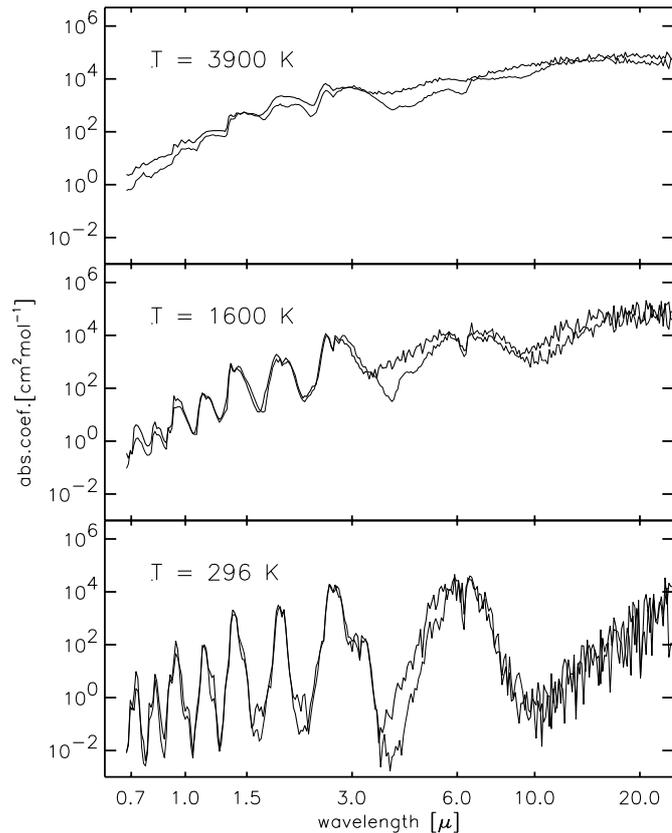

Fig. 5. Comparison of the absorption coefficients calculated based on the NASA AMES line list data (thin lines) and in the present work (thick lines).

The University College London line list (hereafter UCL97; Viti et al. 1997) is based on a method where very accurate frequencies can be achieved, approaching the accuracy commonly obtainable in laboratory measurements. This method has proven very powerful for example for the identification of very high J, high excitation water lines in sun spot spectra (Polyansky et al. 1997). The computing time for this method is very high, and no line list sufficiently complete for stellar opacity calculations is yet available (Viti et al. 1997, and personal communication with J. Tennyson 2000).

6. Effects on stellar atmospheres

Some effects of our computed opacities on the model structure of a cool red giant are seen in Fig. 6, where the temperature as a function of geometrical depth in the atmosphere is shown. The models are computed by use of various fractions of our computed absorption coefficient for H$_2$O, as indicated in the legend, ranging from no H$_2$O opacity included, over all lines with intensity greater than 10^{-3} km mol^{-1} (at 3500 K), to all lines with intensity greater than 10^{-4}, 10^{-5}, 10^{-6}, 10^{-7}, and finally 10^{-20} km mol^{-1}.

It is seen that inclusion of the 50 000 strongest lines (stronger than 10^{-2} km mol^{-1} at 3500 K), which together make up for $\approx 80\%$ of the integrated absorption coefficient,
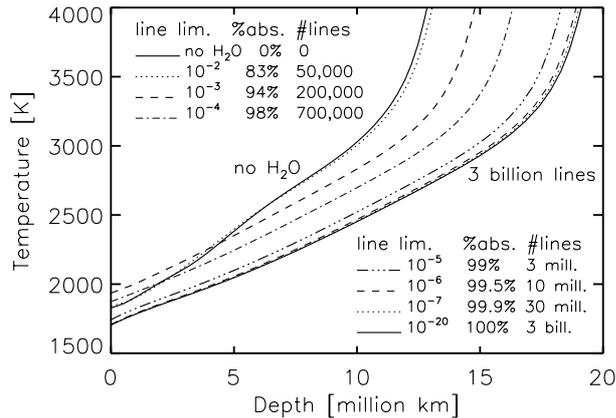
Fig. 6. The temperature as function of geometrical depth in model atmospheres of a red giant star of $T_{eff} = 3000$ K, $\log(g) = 0.0$, $Z = Z_\odot$, and C/O = 0.43. Depth is given in units of 10^6 km, and the surface (depth = 0) is defined as the uppermost computed layer, where $\log(\tau_{Ross}) \approx -5$. The models differ by the completeness of the H$_2$O absorption coefficient included in the opacity. Only lines stronger than the limiting intensity (in km mol^{-1} at 3500 K) indicated with the legend are considered in each model.

has almost no effect on the structure, whereas inclusion of the remaining $\approx 20\%$ of the opacity forces the atmosphere to increase $\approx 50\%$ in size (from 13 to almost 20 million km from atmospheric top to bottom). Note also the great similarity (almost indistinguishability) of the models based on 10 million, 30 million, and 3 billion lines, respectively.

The model atmospheres shown here were computed based on the MARCS code, originally introduced by Gustafsson et al. (1975), and with updates and most of the modifications relevant for the present work being described in Jørgensen et al. (1992) and Jørgensen (1997). In addition to water, the models in Fig. 6 include opacities from TiO, CO, SiO, and OH. If TiO (the other strong absorber in these types of stars) is excluded from the opacity (as in Jørgensen et al. 1994), the effect of inclusion of the weak H$_2$O lines is even more pronounced than shown in Fig. 6. Also for dwarf stars, where the role of TiO relative to H$_2$O is smaller, the effect of the weak H$_2$O lines is bigger than illustrated in Fig. 6.

7. Comparison with stellar spectra

In Fig. 7 we show an observed SWS1 spectrum of the semiregular variable M-type giant star SV Peg, obtained with the Infrared Space Observatory (ISO). Details of this spectrum as well as other cool M-type stars from our ISO observation program will be discussed separately in a second paper (Aringer et al. 2000, in preparation). Together with the observed spectrum is also shown in Fig. 7 a synthetic spectrum, computed from a model atmosphere of $T_{eff} = 2900$ K, $\log g = 0$, $Z = Z_\odot$, and the present line list of H$_2$O (plus the opacity from TiO, CO, SiO, and OH, and with the model and the spectrum computed mutually consistent).
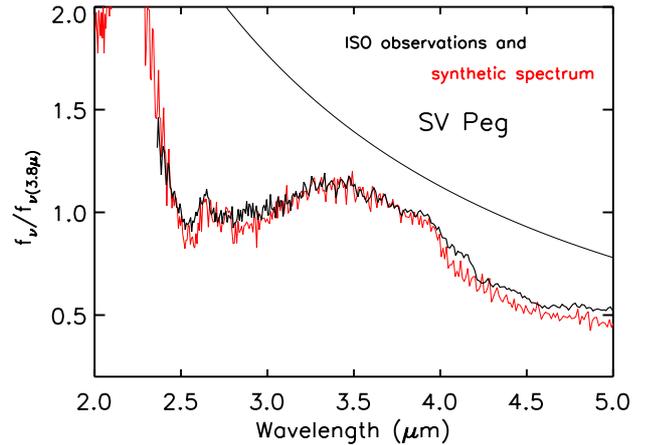

Fig. 7. Comparison of an observed ISO spectrum of the M-type giant SV Peg (thick black line) and our computed spectrum (thin grey line) in the region 2 to 5 μm. Upper convolving line indicate the synthetic continuum flux.

Several vibrational bands of H$_2$O contribute to the observed spectrum in this region. The two strongest ones are the 001 fundamental (centered at 2.66 μm) and the 100 fundamental (centered at 2.73 μm). As noted above, our computed integrated band intensities of these (at room temperature) are 45.4 km mol^{-1} and 2.12 km mol^{-1}, respectively, while the listed values in HITRAN are 43.4 km mol^{-1} and 2.98 km mol^{-1}, respectively. Also several combination bands contribute in this region, the strongest one being the bending vibration first overtone 020 at 3.17 μm, with a calculated and listed intensity of 0.61 km mol^{-1} and 0.456 km mol^{-1}, respectively.

Other molecules than H$_2$O contribute to the absorption in the SWS1 ISO region in M-type stars, too. The most pronounced in the region plotted in Fig. 7 are OH, CO, and SiO. The individual contributions of each of these molecules to the spectrum in Fig. 7 are shown in panels 1 (OH), 2 (CO), and 3 (SiO) (from the top) in Fig. 8, together with the contribution of H$_2$O (lowest panel). All spectra in Fig. 8 are computed based on the same model atmosphere structure, but including only the named species in the spectrum computation. While H$_2$O is the dominant absorber in all of the spectral region plotted, also CO and SiO contribute substantially in the long-wavelength part of the region, and near the short-wavelength edge of the SWS1 spectral capability at 2.3 μm.

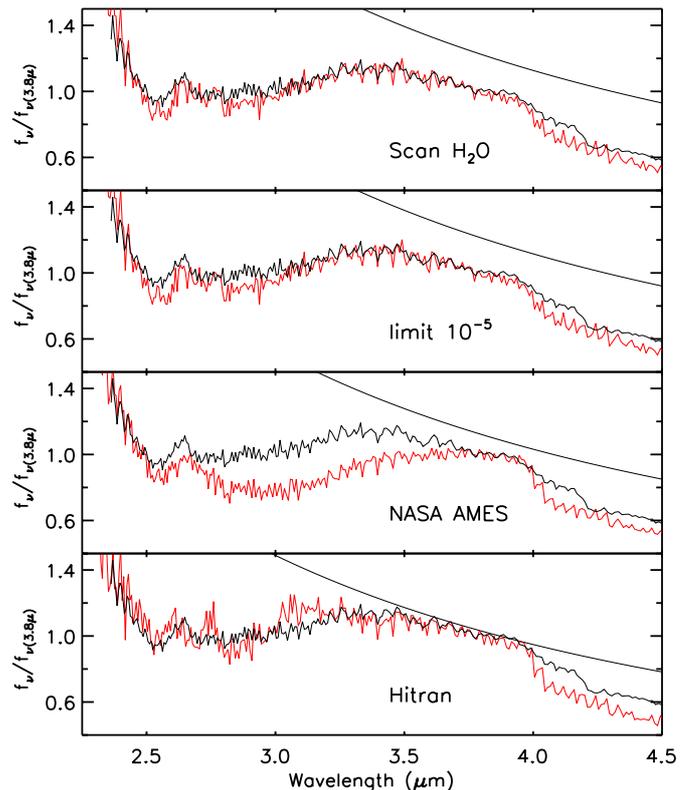In Fig. 9 we show again the ISO spectrum of SV Peg in the 2.3$-$4.5 μm spectral region. From top to bottom in the figure, the panels show in addition to the observed spectrum, the synthetic spectra computed from (1) our present Scan H$_2$O line list, (2) a sub-set of this list consisting only of the lines with an intensity stronger than 10^{-5} km mol^{-1} at 3500 K, (3) the PS97 list, and (4) the HITRAN data base line list. All spectra are calculated from a model atmosphere with the same fundamental parameters as in Figs. 7 and 8, and with the same line data
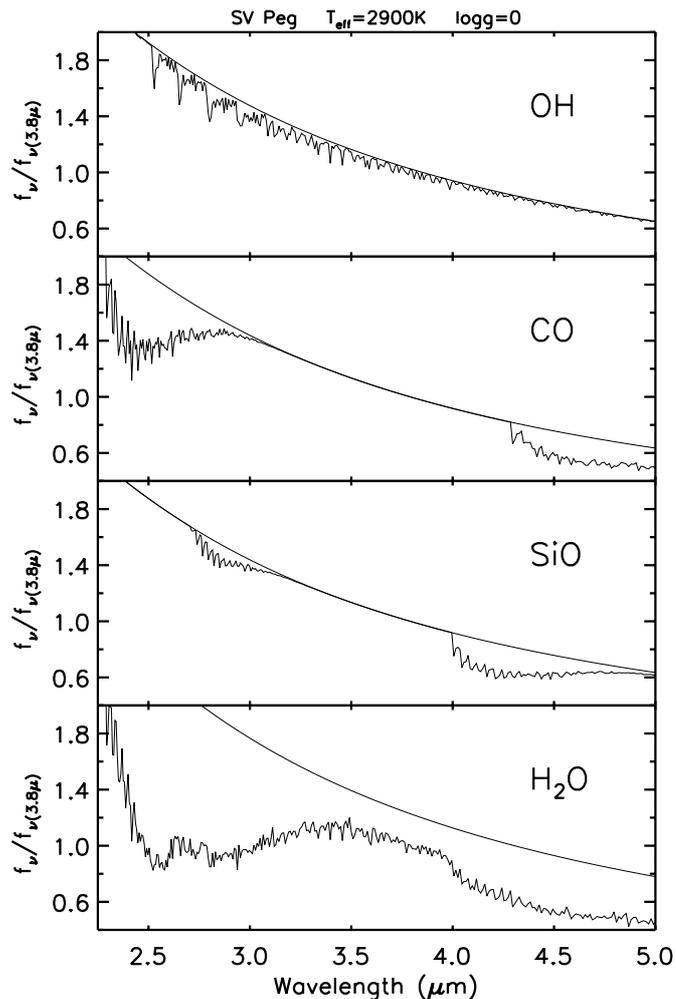
Fig. 8. The separate contribution to the spectrum in Fig. 7 of the absorption from the molecules OH (top panel), CO (second panel from the top), SiO (third panel), and H_2O (bottom panel).

Fig. 9. Synthetic spectra in the 2.3 to 4.5 μm region. The models and spectra are based on the same fundamental parameters as in Figs. 7 and 8, and on the same input data, except for H_2O which from top to bottom in the figure are taken from (1) our full line list, (2) a subset of this list including only lines stronger than 10^{-5} km mol^{-1}, (3) the NASA AMES list, and (5) the HITRAN list, respectively. As in Fig. 7, black curves correspond to the observed spectrum, while the grey lines are the synthetic spectra.

for CO, SiO, OH, and TiO. Only the line lists for water used in the model computations are different among the four panels. The same line lists are adopted for the spectrum computation and the underlying stellar models, such that the spectra and the model atmospheres are mutually consistent.

From the two upper most panels it is recognized that almost the same good agreement between the observed and the synthetic spectrum can be obtained from our full 3-billion-lines list and from the 1 000 times smaller 3-million-lines list with only lines stronger than 10^{-5} km mol^{-1}. The obvious conclusion that 3 million lines are sufficient for model and spectrum computations of cool stars, is not valid because most of the shown region is dominated by two of the strongest water bands. Figures 6 and 9 together do, however, illustrate that for most applications a line list of a few times 10 million lines is more than sufficient if the lines are selected wisely with a selection criterion based on the intensities at high temperature.

Panel 3 (from the top) in Fig. 9 shows the corresponding comparison between the observed spectrum and a spectrum based on the PS97 water line list. The large difference shown in Fig. 5 between our line list and the PS97 list in the 3.5−5 μm region manifests its effect on the spectrum in this panel. The main difference between the two lists was seen from Fig. 5 to be a weaker absorption coefficient in the 4−5 μm region in the PS97 work (as in the HITRAN data) than in our data. The reason that the weaker PS97 absorption coefficient does not show up in Fig. 9 as a weaker 3.5−5 μm band, but rather as a too strong absorption in the PS97 synthetic spectrum in the 2.5−3.5 μm region, is mainly due to the wavelength of normalization. We have chosen in all the spectra shown here to use the same standard normalization at 3.8 μm as in all our previous papers on ISO observations, as first introduced in our paper on R Scl (Hron et al. 1998). The reason for this choice is the absorption minimum at wavelengths in this region, which makes the normalization less dependent on the model structure and input data. If we had chosen to normalize the spectra at shorter wavelengths (e.g. at 3 μm) then the discrepancy between the PS97 synthetic

spectrum and the observed spectrum would have shown up as a flux excess in the PS97 spectrum in the $3.5-5\,\mu$m region instead.

The last panel in Fig. 9 shows the comparison of the observed spectrum with a synthetic spectrum computed based on the HITRAN line list. At first glance the agreement could look surprisingly good. However, several details have to be observed. First, the two flux peaks (at $\approx2.75\,\mu$m and $3.1\,\mu$m) in the synthetic spectrum, relative to the observed spectrum, in the middle of the strong water absorption, bear witnesses to a lack of the veil of weak absorption usually characteristic for a complete high-temperature monochromatic molecular absorption coefficient. Second, and more important, is the almost total lack of absorption in between the main bands, seen in Fig. 9 as a coincidence between the spectrum and the theoretical continuum in the $3.5-4.0\,\mu$m spectral region. This lack of continuum-like molecular line absorption has a strong effect on the model structure and results in stronger bands (and lines) of basically all molecules other than the opacity-dominating species (which is H₂O here).

Because of this effect, in the bottom panel of Fig. 9 the agreement with observations for the SiO fundamental around $4\,\mu$m and the wing of the CO fundamental around $4.5\,\mu$m is worse than in the three other panels. This disagreement will show up even more pronounced elsewhere in the spectrum for trace elements, but it certainly is noteworthy, and hopefully thought-provoking, to see that the less complete HITRAN line list appears at a first glance to be showing better agreement with the observed spectrum than results obtained from the much more complete PS97 list. It also stresses again the important lesson learned several times before (see e.g. Jørgensen 1989), that the gross synthetic spectrum can in principle be in excellent agreement with observations based on a completely wrong model, but that the opacity-weak structures are less likely to look realistic based on a wrong model structure.

8. Conclusions

We have computed the transition moment of all 85 000 vibrational bands due to the water molecule, between vibrational states with energies less than 30 000 cm⁻¹. From this complete set of vibrational transitions, line lists based on various settings of the rotational parameters were constructed and tested, the most complete resulting in 3 billion lines.

The resulting 3 billion lines and various sub-sets of these were used to construct opacity sampling functions, by which the effects on stellar atmospheres were analyzed.

It was shown that the interaction between radiation and the high-temperature gases in a stellar atmosphere is almost entirely by way of the many relatively weak lines with intensities between 10^{-3} and 10^{-5} km mol⁻¹ although they account for only about 10% of the integrated opacity. Lines weaker than $\approx10^{-6}$ km mol⁻¹, although numerous, cause no further change in the computed model atmospheric structure.

There are about 100 million lines stronger than 10^{-9} km mol⁻¹ (at 3500 K), and these were concluded to be more than sufficient for constructing reliable model atmospheres involving the highest temperature gases up to temperatures where the water molecule dissociates. It was shown with an example that a synthetic spectrum with less than 10% of this number of lines was almost indistinguishable from a spectrum based on the 100-million-lines list (or the full 3-billion-lines list). Thus, it was concluded that the 100 million lines would be more than sufficient for all practical purposes, and the corresponding list was included in the Scan data base and made easily available to the community by anonymous ftp (ftp to `stella.nbi.dk`, login as anonymous with email address as password, and then cd to pub/scan). Also two, more easily manageable smaller subsets were placed in the Scan data base, particularly suitable for spectroscopic studies and for planetary atmospheric research.

Finally, the results from using the constructed Scan H₂O line list were tested by comparison with SWS1 ISO spectra of the late type giant star SV Peg. Very good agreement was found between observed and computed spectra, and it was found that results based on our Scan H₂O list were in considerably better agreement with observations than results based on any other available H₂O line list data in the literature.

References

Allard, F., Hauschild, P. H., & Schwenke, D. W. 2000, ApJ, 540, 1005

Auman, J. R. 1967, ApJS, 14, 171

Brown, J. A., Johnson, H. R., Alexander, D. R., Cutright, L. C., & Sharp, C. M. 1989, ApJS, 71, 623

Bunker, P. R., & Jensen, P. 1998, Molecular Symmetry and Spectroscopy, 2nd edition (NRC Research Press)

Duijneveldt, F. B. van 1971, IBM Res. Rep. RJ, 945 A1

Fernley, J. A., Miller, S., & Tennyson, J. 1991, J. Mol. Spectrosc., 150, 597

Gustafsson, B., Bell, R. A., Eriksson, K., & Nordlund, Å. 1975, A&A, 42, 407

Hauschildt, P. H., Allard, F., Ferguson, J., Baron, E., & Alexander, D. R. 1999, ApJ, 525, 871

Hron, J., Loidl, R., Höfner, S., et al. 1998, A&A, 335, L69

Iachello, F., & Oss, S. 1990, J. Mol. Spectrosc., 142, 85

Jensen, P. 1988, J. Chem. Soc. Faraday Trans., 2, 84

Jensen, P. 1989, J. Mol. Spectrosc., 133, 438

Jørgensen, U. G. 1989, ApJ, 344, 901

Jørgensen, U. G. 1995, in Astrophysical Applications of Powerful New Databases, ed. S. J. Adelman, & W. L. Wiese, ASP Conf. Ser., 78, 179

Jørgensen, U. G. 1997, in Molecules in Astrophysics: Probes and Processes, ed. E. F. van Dishoeck (Kluwer), 441

Jørgensen, U. G., & Jensen, P. 1993, J. Mol. Spectrosc., 161, 219

Jørgensen, U. G., & Larsson, M. 1990, A&A, 238, 424

Jørgensen, U. G., Jensen, P., & Sørensen, G. O. 1994, in Poster Session Proceedings of IAU Coll. 146, ed. P. Thejll, & U. G. Jørgensen, Copenhagen University, 51

Jørgensen, U. G., Johnson, H. R., & Nordlund, Å. 1992, A&A, 261, 263

Langhoff, S. R., & Bauschlicher, C. W. 1994, in Molecules in the Stellar Environment, ed. U. G. Jørgensen, Springer LNP, vol. 428, 310

Ludwig, C. B., Malkmus, W., Reardon, J. E., & Thomson, J. A. L. 1973, Handbook Infrared Rad. Combustion Gases, NASA SP-3080

Partridge, H., & Schwenke, D. W. 1997, J. Chem. Phys., 106, 4618

Plez, B., Brett, J. M., & Nordlund, Å. 1992, A&A, 256, 551

Polyansky, O. L., Zobov, N. F., Viti, S., et al. 1997, Science, 277, 346

Roos, B. O., Taylor, P. R., & Siegbahn, P. E. M. 1980, Chem. Phys., 48, 157

Rothman, L. S., Gamache, R. R., Goldman, A., et al. 1987, Appl. Opt., 26, 4058

Rothman, L. S., Rinsland, C. R., Goldman, A., et al. 1998, J. Quant. Spectrosc. Radiat. Transfer, 60, 665

Sarka, K., & Demaison, J. 2000, in Computational Molecular Spectroscopy, ed. P. Jensen, & P. R. Bunker (Wiley), 256

Viti, S., Tennyson, J., & Polyansky, O. L. 1997, MNRAS, 287, 79